DE GRUYTER Open Geosci. 2019; 11:815–828

Research Article

Min Yang*, Ling Han, Youning Xu, Hailing Ke, Ningchao Zhou, Hui Dong, San Liu, and Gang Qiao

Near Infrared Spectroscopic Study of Trioctahedral Chlorites and Its Remote Sensing Application

https://doi.org/10.1515/geo-2019-0063 Received Sep 08, 2017; accepted Apr 03, 2019

Abstract: The mineral chemistry of thirteen trioctahedral chlorite samples from four regions in northwestern China, having a wide range of Fe and Mg contents and relatively constant Al and Si contents, were studied via raman spectroscopy, near infrared (NIR) spectroscopy, Xray diffraction (XRD) analysis and electron - probe microanalysis. Five absorption features of the twenty samples near 4525, 4440, 4350, 4270 and 4180 cm⁻¹ were observed, and two diagnostic features at 4440 and 4270 cm⁻¹ were recognized. Assignments of the two diagnostic features were made for two combination bands $((v+\delta)_{(AlAl)O-OH})$ and $(\nu+\delta)_{(SiAI)O-OH)}$ by regression with Raman fundamental absorptions. Furthermore, the determinant factors of the NIR band position were found by comparing the band positions with relative components. The results showed that $Fe^{2+}/(Fe^{2+}+Mg)$ values are negatively correlated with the two NIR combination bands. The findings provide an interpretation of the NIR band formation and demonstrate a simple way to use NIR spectroscopy to discriminate between chlorites with different components. More importantly, a simple example of mapping Fe-rich and Mg-rich chlorites were executed using remote sensing data based on this theory. The spectroscopic detection of mineral chemical variations in chlorites provides geologists with a tool with which to collect information on hydrothermal alteration zones from hyperspectral-resolution remote sensing data.

Keywords: chlorite; near infrared spectroscopy; Raman spectroscopy; micro-X-ray diffraction; fundamental vibration; combinational vibration; electron - probe microanalysis

Ling Han, San Liu: School of Earth Science and Resources, Chang'an University, Xi'an 710061, China

1 Introduction

Chlorites are ubiquitous ferromagnesian phyllosilicates most commonly found in epimetamorphic rocks as hydrothermal alteration products and after erosion in sediments together with various clay minerals [1, 2]. The crystal structure of the chlorite group minerals can be described as a 2:1-type hydrous aluminosilicate (talc-like layer) with the octahedral sheet "sandwiched" between two opposite tetrahedral sheets and linked by an extra octahedral sheet (brucite-like layer). The simplified structural formula of chlorite minerals can be described as $Mg_6Mg_6(Si_8O_{20})(OH)_4(OH)_{16}$, in which sheets of talc $(Mg_6(Si_8O_{20})(OH)_4)$ and brucite $(Mg_6(OH)_{12})$ are included (Figure 1). The brucite-like and talc-like sheets are bonded to one another by long hydrogen bonds between the oxygen atoms from the siloxane sheet of the talc-like layer and the hydroxy groups of the brucite-like layer. Cation substitution is very common in chlorites and leads to a wide range of chemical compositions. In some cases, partial substitution of the Mg²⁺ by Fe³⁺ occurs in the brucite-like layers accompanied by a coupled charge compensation, whereas substitution of Si⁴⁺ by Al³⁺ occurs in the tetrahedral sheet of the talc-like layer. These substitutions produce a variety of clinochlore with a structural formula of $Mg_4Al_2Mg_6(Si_6Al_2O_{20})(OH)_4(OH)_{12}$. The presence of Al in both the octahedral and tetrahedral sheets is necessary to ensure similar crystal cell parameters for the formation of a stable structure. Mg²⁺ can also be replaced by Fe²⁺, leading to a type of Fe-rich chlorite known as ripidolite with a theoretical formula of $(Fe^{2+},Mg)_3Al_3(Fe^{2+},Mg)_6(Si_5Al_3O_{20})(OH)_4(OH)_{16}$ [3].

a

Most of the available vibrational spectral studies have focused on the infrared, Raman and other vibrational spectra of chlorites, and some correlations between spectral features and chemical composition have been published.

Youning Xu, Hailing Ke, Hui Dong, Gang Qiao: Xi'an Centre of China Geological Survey, Xi'an 710054, Shaanxi, China Ningchao Zhou: Key Laboratory for Geohazards in Loess Areas, Chinese Ministry of Natrual Resources, Xi'an 710054, Shaanxi, China

^{*}Corresponding Author: Min Yang: Key Laboratory for Geohazards in Loess Areas, Chinese Ministry of Natrual Resources, Xi'an 710054, Shaanxi, China; Xi'an Centre of China Geological Survey, Xi'an 710054, Shaanxi, China; School of Earth Science and Resources, Chang'an University, Xi'an 710061, China; Email: ymin@cgs.cn

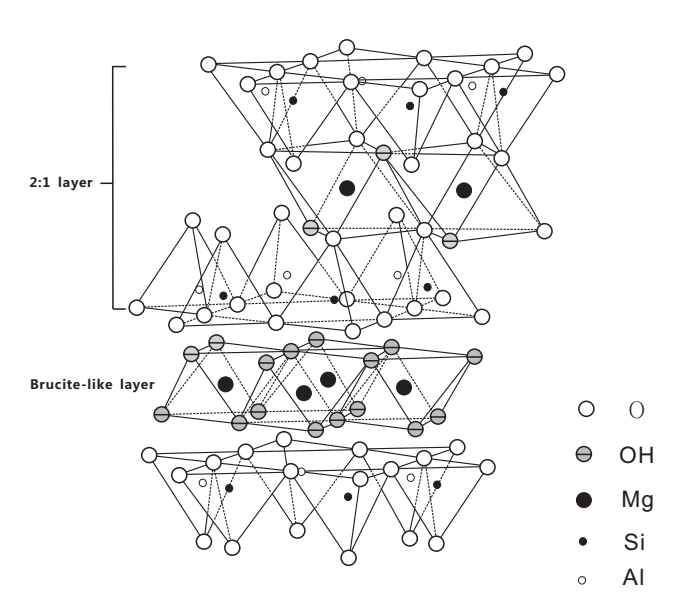


Figure 1: The structure of chlorite. Brucite-like and 2:1 layers are contained in the structure.

Tuddenham and Lyon (1959) [4] observed the relationship between the substitution amount of Al for Si in the tetrahedral positions and the wavenumber of the Si-O stretching. In addition, Stubican and Roy (1961) [5] stated that the substitution of Al for Si was closely related to the position of the strongest Si-O band in the 665 to 685 cm⁻¹ region. Hayashi and Oimuma (1967) [6] reported a band shift from 540 to 560 cm⁻¹ with an increasing octahedral Al content but an opposite shift with increasing Mg and Fe contents. Moreover, Hayashi and Oinuma observed a shift toward lower frequencies of the band between 620 and 692 cm⁻¹ with increasing octahedral Mg and Fe and decreasing octahedral Al content. Additionally, they observed another shift toward lower frequency in the OH stretching bands from 3400 to 3436 cm⁻¹ and from 3560 to 3586 cm⁻¹ with increasing Fe content. These shifts in OH stretching bands were interpreted as being due to a shorter -OH interlayer distance in Fe-rich chlorites. The two broad bands near 3560 and 3420 cm⁻¹ were ascribed to the interlayer OH with a weak shoulder band around 3620 cm⁻¹ associated with the inner OH of the 2:1 sheet [7]. The two relatively strong bands were generally assigned to the (SiAl)O-OH and (AlAl)O-OH vibrations [8], and the intensities were mainly determined by the tetrahedral sheet composition, while the exact band positions were also related to the composition of the octahedral interlayer hydroxide sheet.

The near infrared (NIR) spectra of chlorites have also been studied by some researchers, but they mostly focused on the application of NIR spectra to discriminate chlorites from other minerals. J. L. Post (2014) [9] observed a shift in the overtone band from 7102 cm⁻¹ to 7205 cm⁻¹ and sug-

gested that this shift might make the identification of chlorite by remote sensing more difficult. Min Yang (2014) [10] and K. Laakso (2016) [11] observed a hydroxyl absorption shift (4424 cm⁻¹ to 4456 cm⁻¹) toward higher frequency with increasing Mg and toward lower frequency with increasing Fe, but they did not discuss the hydroxyl absorption band near 4273 cm⁻¹. S. Petit (2015) [12] assigned the NIR features of octahedral smectites (2:1 layer) near 4550 cm⁻¹ and 4370 cm⁻¹ to the combination of hydroxyl stretching and bending modes. As with the layer minerals of 2:1, the NIR features of chlorites may also be related to the combination of hydroxyl stretching and bending in the octahedral sheet.

Raman studies and NIR studies are historically distinct from one another. The former have mainly focused on functional groups and spectral interpretation, whereas the latter have focused on statistical analysis. The use of spectral units of cm⁻¹ (wavenumber) in Raman and nm (wavelength) in NIR is symptomatic of the historical divide separating these research communities.

The aim of this paper is to compare NIR data with Raman data with respect to the Fe²⁺/(Fe²⁺+Mg) values and identify changes that occur in the NIR spectra as a function of the Raman features and cation substitutions. The NIR reflectance technique, which is particularly fast and efficient for identifying both minerals bearing hydroxyl moiety and carbonate minerals, would contribute to detecting the gossans and hydrothermal products on the earth's surface when mapping the land using multi- or hyperspectral remote sensing [13].

2 Materials and Methods

2.1 Samples

Electron - probe microanalysis, Raman, NIR and XRD data for thirteen samples were collected from the four regions in northwestern China (Table 1). The samples were cut, polished and made into thin sections, 30 microns in thickness. The thin sections were used for Micro area XRD analysis, Electron - probe microanalysis and Raman spectra collection. NIR spectra were collected on the rock samples and for further spectral analysis. The mineral component data of these thirteen samples determined by electron – probe microanalysis were used to elucidate the relationship between spectral features and certain components by comparing the Raman and NIR band positions.

 Table 1:
 Chemical composition of chlorite samples collected from four regions in this study.

	XH-02	XH-04	XH-05	XH-10	XH-17	XH-20	QH-01	QH-08	TJ-02	Y-07	KD-04	QL-04	QL-05
		Beis	nan area in	Beishan area in Gansu Province	nce			Nachitai in		West Kunlun area	ılun area	Qinling	g area
							_	Qinhai Provin	ce	in Xinjian§	g Province	in Shaanx	i Province
SiO ₂	29.86	27.24	28.69	28.24	27.71	28.59	26.22	27.75	26.23	25.00 2	25.90	26.32	26.87
TiO ₂	0.00	0.00	0.03	0.03	0.03	0.05	0.07	0.05	0.00	0.02	90.0	0.01	0.05
Al_2O_3	17.19	20.14	18.52	18.16	19.91	17.97	21.95	18.49	18.21	22.13	22.24	19.93	18.91
Cr_2O_3	0.02	0.07	90.0	0.01	0.04	0.02	0.10	0.04	0.00	0.02	0.08	0.01	0.10
Fe0	24.02	21.81	20.62	22.09	21.98	23.15	19.96	25.39	28.17	22.30	26.14	26.97	23.89
MnO	0.37	0.40	0.31	0.48	0.24	0.29	0.24	0.40	0.28	0.30	0.16	0.39	0.37
NiO	0.05	0.03	0.03	0.00	0.01	0.00	0.02	0.09	0.00	0.00	0.00	90.0	0.09
MgO	18.19	17.66	19.21	19.66	18.67	18.36	18.49	16.53	14.10	17.29	12.80	14.59	16.87
Ca0	0.09	0.04	0.03	0.00	00.0	0.02	0.01	0.01	0.01	0.02	0.02	0.00	0.09
Na_2O	0.00	0.00	0.01	0.01	00.0	0.01	0.00	0.05	0.01	0.01	0.04	0.02	0.00
K ₂ 0	0.02	0.00	0.00	0.00	0.01	0.20	0.00	0.14	0.03	0.01	0.00	0.04	0.00
H ₂ 0	11.80	11.57	11.68	11.72	11.74	11.66	11.64	11.53	11.09	11.46	11.34	11.36	11.38
Total	101.59	98.97	99.21	100.42	100.34	100.30	98.70	100.45	98.12	98.57	98.79	99.70	98.61
Si	3.05	2.84	2.96	2.92	2.84	2.95	2.71	2.89	2.83	2.61	2.77	2.78	2.83
=	0.00	0.00	0.00	0.00	0.00	0.00	0.01	0.00	0.00	0.00	0.01	0.00	0.00
Al ^{IV}	0.95	1.16	1.04	1.08	1.16	1.05	1.29	1.11	1.17	1.39	1.23	1.22	1.17
Al ^{VI}	1.13	1.31	1.22	1.15	1.24	1.13	1.39	1.15	1.15	1.33	1.58	1.27	1.18
ڻ	0.00	0.01	0.00	0.00	0.00	0.00	0.01	0.00	0.00	0.00	0.01	0.00	0.01
Fe ³⁺	0.00	0.00	0.00	0.00	0.00	0.00	0.00	0.00	0.02	90.0	0.00	0.00	0.00
Fe ²⁺	2.05	1.90	1.78	1.94	1.88	1.99	1.73	2.21	2.52	1.89	2.34	2.38	2.11
Wn	0.03	0.04	0.03	0.03	0.02	0.02	0.02	0.03	0.03	0.03	0.01	0.04	0.03
ï	0.00	0.00	0.00	0.00	0.00	0.00	0.00	0.01	0.00	0.00	0.00	0.01	0.01
Mg	2.77	2.74	2.96	2.87	2.85	2.82	2.85	2.56	2.27	2.69	2.04	2.30	2.65
ප	0.01	0.00	0.00	0.00	0.00	0.00	0.00	0.00	0.00	0.00	0.00	0.00	0.01
Na	0.00	0.00	0.00	0.00	0.00	0.00	0.00	0.01	0.00	0.00	0.01	0.00	0.00
¥	0.00	0.00	0.00	0.00	0.00	0.03	0.00	0.02	0.00	0.00	0.00	0.01	0.00
$Fe^{2+}/(Mg+Fe^{2+})$	0.43	0.41	0.38	0.40	0.40	0.41	0.38	0.46	0.53	0.41	0.53	0.51	0.44
Al ^{IV} /(Al ^{IV} +Si)	0.27	0.32	0.29	0.28	0.30	0.28	0.34	0.29	0.29	0.34	98.0	0.31	0.29
Tot. Cat.	10	10	10	10	10	10	10	10	10	10	10	10	10

2.2 Micro area XRD analysis

Thirteen samples from the four regions were cut into small pieces ($24\times30\times0.03$ mm) and polished, and then analyzed with a D/MAX rapid II micro X-ray Diffraction Spectrometer at room temperature using Cu K\$\alpha\$ radiation at 40 kV and 300 mA (State Key Laboratory for Mineral Deposits Research, Nanjing University). The spot size is approximately 50 \mum. Analyses were performed on areas of 50 to 100 \mum diameter in the chlorite crystals. X-ray diffraction patterns were smoothed slightly and backgrounds were subtracted using Jade 6.0 software [14, 15].

2.3 NIR spectroscopy

All NIR spectra were obtained using a PANalytical ASD FieldSpec Pro[®] 3 spectrometer (hereafter referred as ASD) that records spectra from the 350 to 2500 nm wavelength (4000 to 28,571 cm⁻¹) region with a spectral resolution of 10 nm and a sampling interval of 1 nm in the shortwave infrared (1300-2500 nm) region. The spectrometer was connected to a contact probe with an internal halogen bulb, which ensures stable illumination conditions during data collection. The raw values of at-sensor radiance were converted to surface reflectance values using a Spectralon™ reflectance panel (i.e., the "white reference," SRT-99-100, Labsphere, Inc., North Sutton, New Hampshire), which is a commercially available plate made of polytetrafluoroethylene [16]. Finally, these relative reflectance values were converted to absolute reflectance values by multiplying the relative reflectance value for each wavelength with the reflectance factor obtained from the calibration certificate of the Spectralon™ panel, in accordance with the procedure of Clark et al. (2002) [17]. The wavelengths of the spectra were converted to wavenumbers to facilitate the comparison with the Raman data.

2.4 Raman spectroscopy

Raman spectra were acquired on the same location of the thin section samples using a Renishaw inVia Raman spectrometer equipped with a microconfocal system. An argon ion laser from Spectra Physics, which was set at a wavelength of 514.5 nm and 5 mw, was used to excite Raman scattering. The spot size was about 2 μm . Peak positions were calibrated against a silicon standard. Two regions from 350 to 1200 cm^{-1} and from 3000 to 3800 cm^{-1} were used for spectral analysis in this study.

2.5 Electron - probe microanalysis

The elemental compositions of the thirteen samples were measured on the same spots from which XRD and Raman data were collected; this experiment was done using a JXA-8230(4CH) electron microprobe (EMP) at the Key Laboratory for Geo-hazard in Losses Area, Ministry of Natural Resources (Xi'an, China) with a 15 kV accelerating voltage, 10 nA sample current, and beam diameters of 5µm. Peak counting times were 10 s, backgrounds were counted 5 s. Standards used included the following synthetic and natural minerals: jadeite (Na, Al), albite (Si), periclase (Mg), NiO (Ni), hematite (Fe), apatite (Ca), Cr₂O₃ (Cr), microcline (K), pyrophanite (Ti, Mn). The raw intensity data were corrected with the 'ZAF' program. The formulas of the clinochlores listed in Table 1 under the oxide results were corrected assuming ten cations according to the theory of Droop in 1987 [18].

2.6 Spectral component analysis

Spectral manipulation, which included baseline adjustment, smoothing and normalization, was processed using the program written by VBA in Microsoft Excel software. The absorption features of chlorites located between 2250 and 2340 nm (4440 and 4270 cm⁻¹) can be explicitly separated into their constituent absorption bands using the Gaussian-Lorentz Model [19], and the mathematical shape description of the individual absorptions is accurate. The Gaussian-Lorentz Model was developed and validated by empirical studies of isolated vibration absorption bands in both transmission and reflectance spectra of autunites, nontronites and smectite [20, 21]. The Gaussian-Lorentz Model fitting was undertaken until reproducible results were obtained with an R² of greater than 0.995.

3 Results

3.1 Micro area XRD analysis

Figure 2 shows full Micro-XRD patterns of the thirteen samples. The minerals including chlorite, albite and quartz are the main component of the samples. The crystal sizes of the clinochlore mineral are mainly between 50 and 100 μm and it is hard to collect the spectra of pure clinochlore.

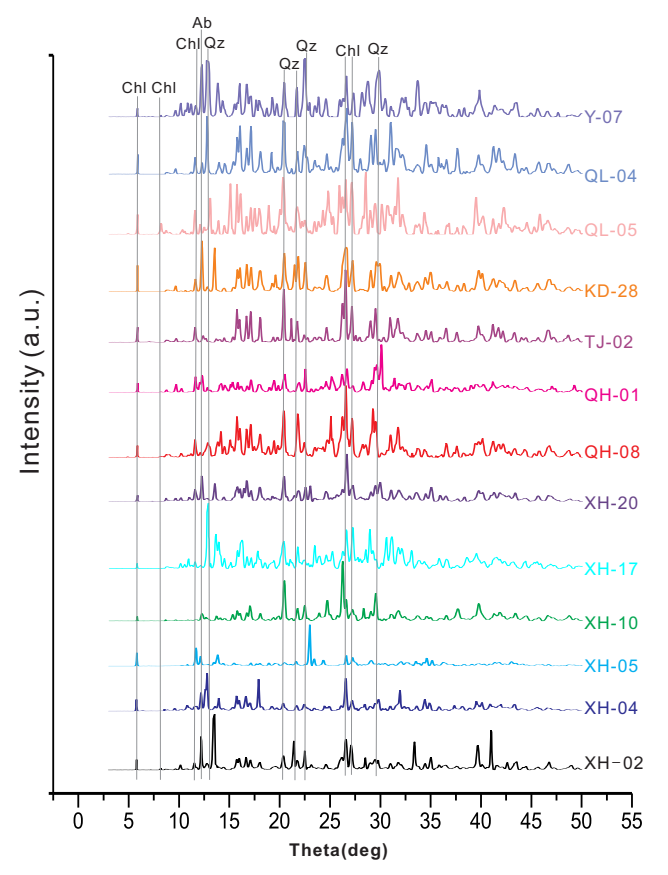


Figure 2: Micro XRD spectra of clinochlore samples, Chl: chlorite, Ab: Albite, Qz: quartz.

3.2 Raman bands

The Raman spectra in this study are perform Si-O absorption bands at approximately 1070 and 1030 cm⁻¹, and these features are not related to NIR spectra [22]; they are therefore not mentioned in the following discussion.

3.2.1 Bands in the $3800-3000 \text{ cm}^{-1}$ spectral range

The Raman spectra ranging from 3000-3800 cm⁻¹ are shown in Figure 3 and Table 2 shows comparisons with some chlorite minerals reported in the literature in order to assist with the assignment of the observed bands for chlorite spectra. A relatively strong band was observed in the Raman spectra near 3650 cm⁻¹, which also occurred on the spectra of talc and was attributed to the stretching of OH groups from the 2:1 layer [23, 24]. Two additional wide absorptions occurred from approximately 3570 to 3442 cm⁻¹ and were also strong and overlapping in large widths at half height. Raman spectra showed an increase in frequency of these bands for the Fe-Mg substitution at constant Al/(Al+Si) and a stable frequency for Al-Si

substitution at constant Fe²⁺/(Fe²⁺+Mg). The bands that occurred near 3570 cm⁻¹ were assigned to the hydroxyl stretch in (AlAl)O-OH ($\nu_{(AlAl)O-OH)}$), and the bands that occurred near 3442 cm⁻¹ were assigned to (SiAl)O-OH stretching ($\nu_{(SiAl)O-OH)}$) [25, 26]. Furthermore, Prieto (1991) [27] observed that an increase of Fe content induced a shift of these two bands toward lower frequency. This relationship was also validated using the Raman spectra in this study, as shown in Figure 4.

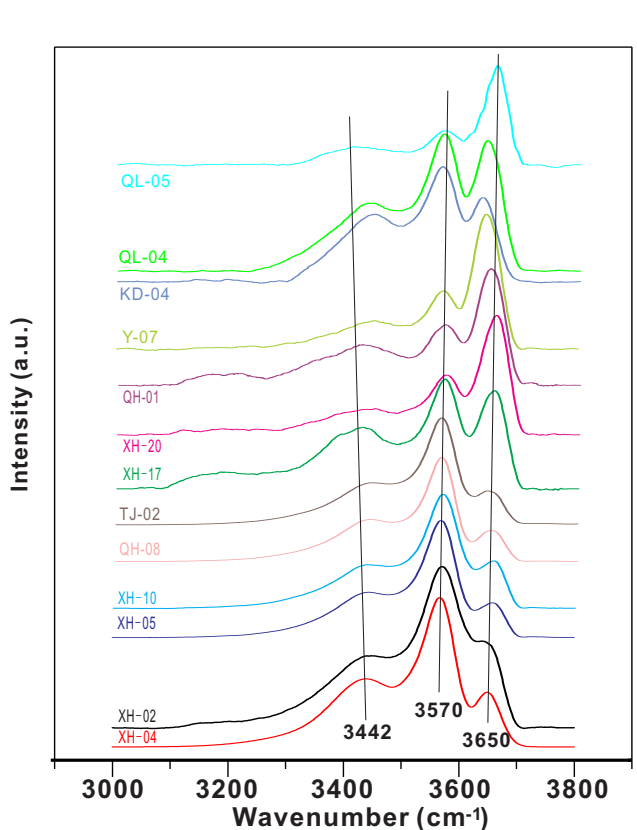


Figure 3: Raman spectra of stretching vibrations of hydroxyl groups in the $3000\text{-}3800~\text{cm}^{-1}$ spectral range. The band positions of 3650, 3570 and $3442~\text{cm}^{-1}$ are the average values from the Raman spectra shown in this plot.

3.2.2 Bands in the 1200-150 cm⁻¹ spectral range

The Raman spectra of the thirteen samples collected from the four regions displayed two intense bands at 1060 and 1030 cm⁻¹ (Figure 5 and Table 2). These bands were assigned to Si-O stretching in 2:1 layers [13, 26] and were also

820 — M. Yang et al. DE GRUYTER

Table 2: Comparison of the Raman spectra used in this study with IR, IES (infrared emission spectra) and Raman spectra from other chlorite studies.

Raman (this study)	IR (Kloprogge 2000)	IES (Kloprogge 2000)	Raman (Prieto 1991)	Assignment
432	435		438	(Fe,Mg)-O-Si bend
472	459		466	v_3 Si-O
555	544	541	548	Al-O-Si
670	653	667	659	v_2 Si-O
770	760	759	775	(SiAl)O-OH bend
877	818	802	814	(AlAl)O-OH bend
	904	885	903	OH bend
	943	925		Inner OH bend
1030	1030	1034	1033	Si-O stretch
1060	1150	1086	1094	Si-O stretch
3442	3419	3450	3462	(SiAl)O-OH stretch
3570	3553	3560	3585	(AlAl)O-OH stretch
3650	3635	3645	3665	Inner OH stretch

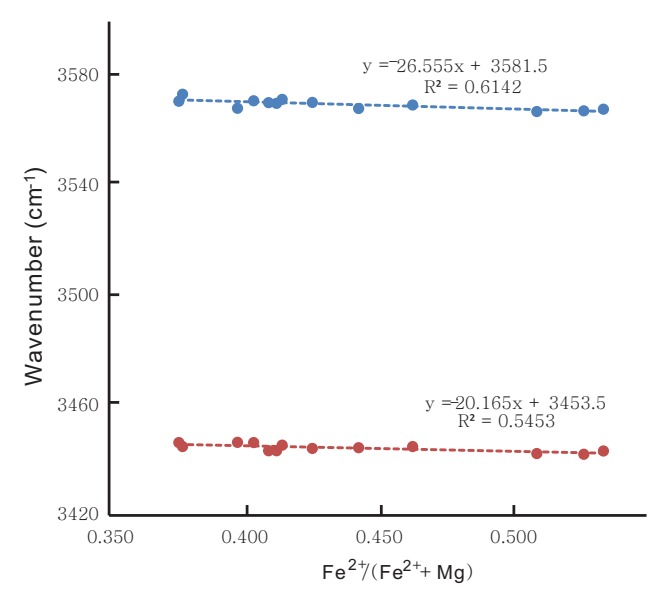


Figure 4: Correlation between the chlorite fundamental bands and $Fe^{2+}/(Fe^{2+}+Mg)$ values.

observed in other phyllosilicates with 2:1 layers [27, 28]. The second type of absorption in this region was located at approximately 877, 770 and 670 cm $^{-1}$. These bands were assigned to (AlAl)O-OH, (SiAl)O-OH and (SiSi)O-OH bending absorptions ($\delta_{(AlAl)O-OH}$, $\delta_{(SiAl)O-OH}$ and $\delta_{(SiSi)O-OH}$), respectively [13, 29]. The frequency of 877 cm $^{-1}$ bands shifted toward higher frequency with an increasing Fe content. In the 400-550 cm $^{-1}$ region, the Raman spectra displayed three bands near 555, 472 and 432 cm $^{-1}$. These bands were assigned to (Fe,Mg)-O-Si or Al-O-Si bending [26].

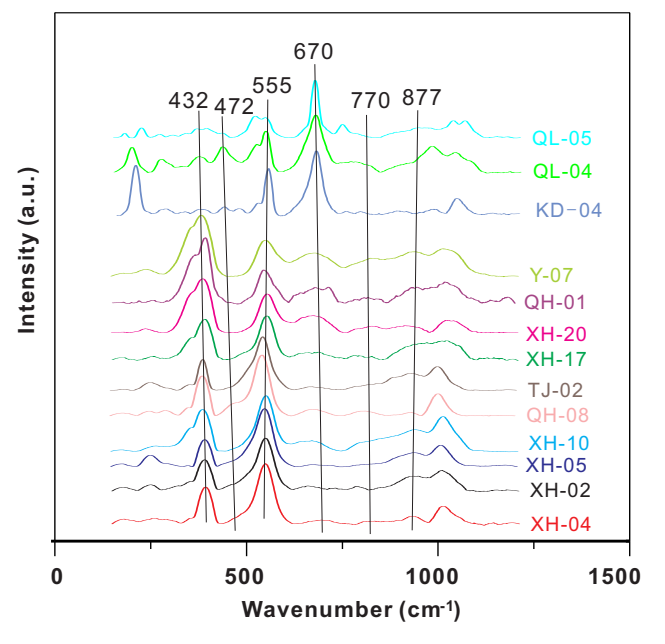


Figure 5: Raman spectra of bending vibrations of hydroxyl groups in the 150-1200 cm⁻¹ spectral range. The band positions are the average values from the Raman spectra shown in this plot.

3.3 NIR bands

For many natural phyllosilicates, the $(\nu + \delta)_{OH}$ combination bands occurring in the NIR region are broad and overlapping (Figure 6). In the spectral component analysis, five independent bands were observed at approximately 4522, 4440, 4338, 4263 and 4175 cm⁻¹ (2211, 2252, 2305, 2345 and 2395 nm), which are the average band positions of all thirteen samples. The two typical samples (XH-20 and QH-01), including 5 independent absorption bands, are shown in

Figure 7. The weak band near 4541 and 4514 cm⁻¹ were assigned to the combination of OH stretching and deformation vibrations of Al-OH groups in 2:1 layers, and this band was also observed at a similar frequency in kaolinites [30]. Another weak band from 4317 to 4353 cm⁻¹ was tentatively attributed to an Mg-OH combination band [10]. The absorptions near 4440 and 4263 cm⁻¹ are intense and have been successfully used to detect chlorites in using remotely sensed data as diagnostic feature [31, 32]. The two absorption features occurred from 4424 to 4451 cm⁻¹ and from 4240 to 4298 cm⁻¹. The band at 4440 cm⁻¹ was closely related to the fundamental bands at 3570 and 877 cm⁻¹, and positive linear correlations were established between the NIR band at 4440 cm⁻¹ and fundamental bands at 3570 and 877 cm⁻¹ following the regressions shown in Figure 8ab. These regressions indicated that the NIR $(v+\delta)_{OH}$ band (hydroxyl combination band) near 4440 cm⁻¹ could be assigned to the combination of (AlAl)O-OH stretching $(
u_{(AlAl)O-OH})$ and (AlAl)O-OH bending $(\delta_{(AlAl)O-OH})$ in the Raman spectra. The absorption of the band at 4263 cm⁻¹ was likely related to the fundamental bands at 3442 and 770 cm⁻¹. Another two positive correlations existed between the NIR band at 4263 cm⁻¹ and Raman bands at 3442 and 770 cm⁻¹, as shown in Figure 8cd. These regressions illustrated that the frequency of the NIR $(v+\delta)_{OH}$ band near 4263 cm⁻¹ could be induced by the combination of (SiAl)O-OH stretching ($v_{(SiAl)O-OH}$) and (SiAl)O-OH bending modes $(\delta_{(SiAI)O-OH}).$

The energy required for the combination band is the sum of the stretching and bending bands in the case of evenly spaced energy levels. Although the wavenumber is proportional to the energy, the combination band should occur at the wavenumber of the sum of the stretching and bending fundamentals. However, due to the anharmonic feature of vibrations, the combination bands appear at a wavenumber that is higher than the sum of the fundamental bands [33]. The observed NIR band assignments are commonly determined by analogy with the fundamental ν_{OH} and δ_{OH} bands [22, 30]. Nevertheless, to interpret spectra, researchers often need to establish a relationship that allows them to estimate the wavenumbers of the combination bands in the NIR from the wavenumbers of the fundamentals (v_{OH} and δ_{OH}) in the IR and vice versa [34]. The anharmonicity constant X, which is determined by the nature of the oscillator and may be affected by the hydroxyl environment (formation of hydrogen bonds, cations, intermolecular interactions, electronegativity, etc.), is calculated with the following equation [35]:

$$X = (\nu + \delta)_{OH} - \nu_{OH} - \delta_{OH} \tag{1}$$

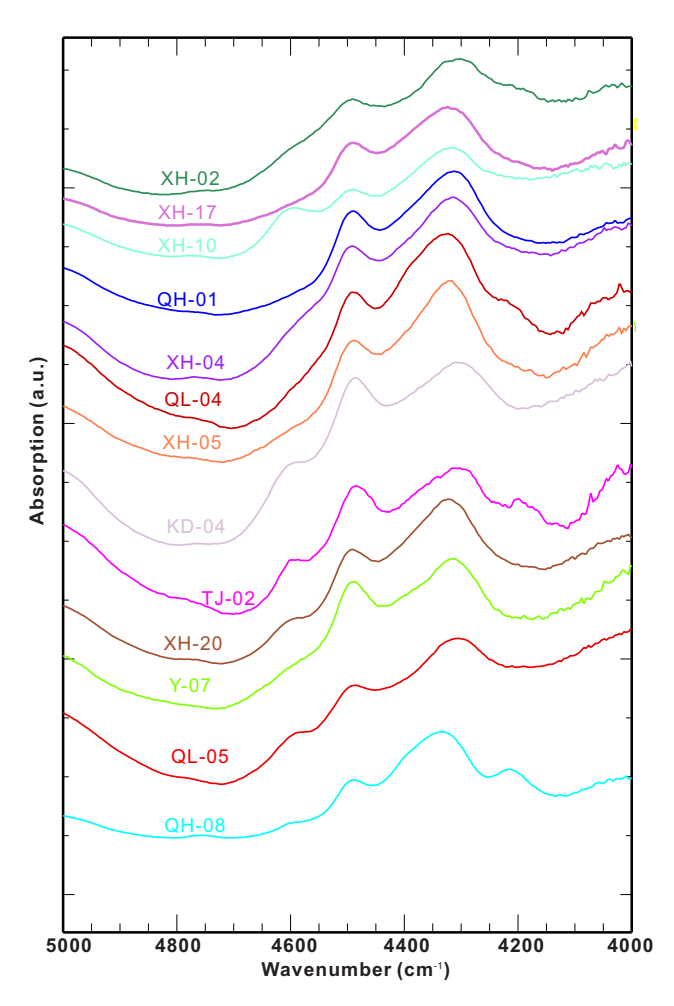


Figure 6: Near infrared spectra of clinochlores in the 4000 to 5000 $\,\mathrm{cm}^{-1}$ region.

Where $(\nu+\delta)_{OH}$ is the wavenumber of the combination band in the NIR region and ν_{OH} and δ_{OH} are the wavenumbers of the stretching and bending bands, respectively, in the IR region. The values of the anharmonicity constant X are calculated from the frequencies (wavenumbers) of the fundamental vibration and the combination vibration for the same OH group (Table 3). The anharmonicity constant values of the 4440 cm⁻¹ band range from -21.58 to 8.54 cm⁻¹, with a mean value of -11.24 cm⁻¹. The anharmonicity constant values of the 4263 cm⁻¹ band range from 31.96 to 65.31 cm⁻¹, with a mean value of 48.47 cm⁻¹.

From Eq. (1), the relations between a combination band ($(v+\delta)_{OH}$) and the fundamental bands (v_{OH} and δ_{OH}) are as follows:

$$(\nu + \delta)_{(AlAl)O-OH} = \nu_{(AlAl)O-OH} + \delta_{(AlAl)O-OH}$$
(2)
+ $X_{(AlAl)O-OH}$

$$(\nu + \delta)_{(SiAl)O-OH} = \nu_{(SiAl)O-OH} + \delta_{(SiAl)O-OH}$$
 (3)
+ $X_{(SiAl)O-OH}$

Table 3: Wavenumbers (in cm $^{-1}$) of the v_{OH} , δ_{OH} and $(v+\delta)_{OH}$ bands observed for chlorites by Raman and NIR methods and calculated values of the anharmonicity constant X.

	$\delta_{ m (AIAI)0-0H}$	$V_{(A1A1)0-0H}$	$(\nu+\delta)_{({ m AIAI})0-0{ m H}}$	$X_{(A1A1)0-0H}$	$oldsymbol{\delta}_{ ext{(SiAl)0-OH}}$	$V_{\rm (SiAl)0-OH}$	$(\nu+\delta)_{(\mathrm{SiAl})0-0\mathrm{H}}$	$X_{(SiAI)O-OH}$
XH-02	864.21	3570.55	4439.46	4.7	763.64	3444.45	4265.21	57.12
XH-04	889.86	3570.43	4441.52	-18.77	787.18	3443.56	4262.7	31.96
XH-05	889.99	3570.99	4440.81	-20.17	772.88	3446.54	4267.53	48.11
XH-10	893.67	3571.16	4443.25	-21.58	762.52	3446.56	4263.74	54.66
XH-17	883.37	3568.43	4439.93	-11.87	781.27	3446.66	4267.51	39.58
XH-20	891.53	3571.65	4441.82	-21.36	776.71	3445.66	4270.54	48.17
QH-01	887.99	3573.53	4442.61	-18.91	778.25	3445.12	4263.19	39.82
QH-08	884.21	3569.62	4438.95	-14.88	778.34	3445.09	4266.49	43.06
TJ-02	860.83	3567.48	4436.85	8.54	756.55	3442.31	4254.78	55.92
Y-07	888.47	3570.18	4439.27	-19.38	771.64	3443.6	4264.6	49.36
KD-04	883.45	3568.06	4438.63	-12.88	749.12	3443.52	4257.95	65.31
QL-04	865.91	3567.26	4438.53	5.36	760.58	3442.52	4258.41	55.31
QL-05	874.59	3568.37	4437.98	-4.98	774.23	3444.68	4260.62	41.71
Mean value				-11.24	Mean value			48.47

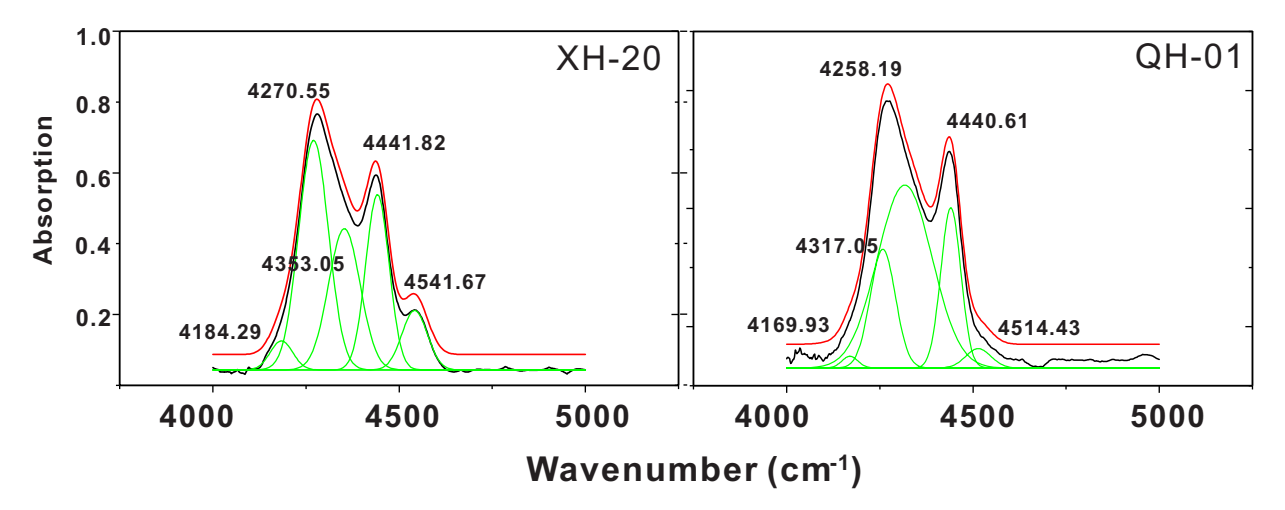


Figure 7: Decomposition of the NIR combination band of chlorites (HL-01 and HL-13). Red line: experimental; black line: fit and diagnostic bands; gray line: fit and not diagnostic bands.

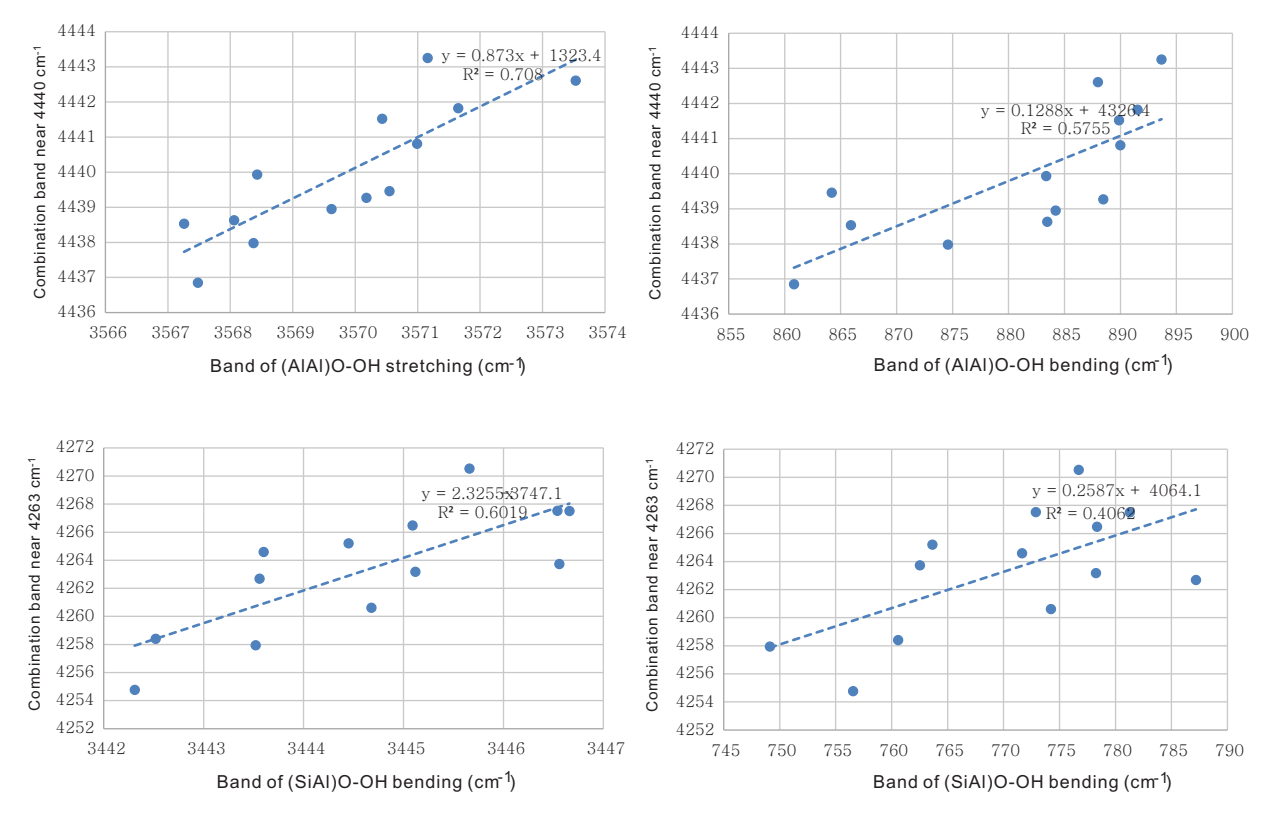


Figure 8: Linear relationships between NIR bands and IR bands.

All along the chemical series, the $(\nu + \delta)_{OH}$ combination bands shifted progressively from 4436.58 cm⁻¹ to 4442.61 cm⁻¹ and from 4254.78 cm⁻¹ to 4270.54 cm⁻¹. Figure 9 shows two direct linear correlations between band position and Fe²⁺/(Fe²⁺+Mg) values for the thirteen chlorite samples collected from the four regions, and this relationship indicated that both absorptions observed in the NIR region shifted toward higher frequency as the Fe²⁺/(Fe²⁺+Mg) value decreased.

These correlations revealed that the Mg-Fe substitution would be the dominant factor in NIR band positions [36]. In other words, the band positions of the two diagnostic combination bands could be used to discriminate among different chlorites with a variety of Fe-Mg contents. As Foster (1962) reported [38], chlorites with higher Fe²⁺/(Fe²⁺+Mg) values (>0.45) would be brunsvigite and those with lower values (<0.45) would be clinochlore and pycnochlorite. Assuming that the absorption coefficients

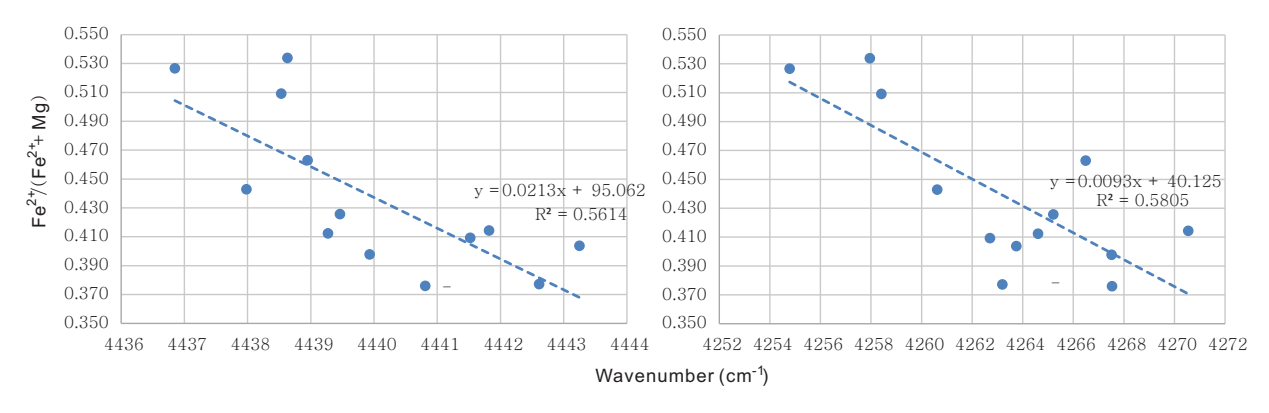


Figure 9: Linear relationships between diagnostic NIR bands (a shows the band near 4440 cm⁻¹, and b shows the band near 4263 cm⁻¹) and $Fe^{2+}/(Fe^{2+}+Mg)$ value.

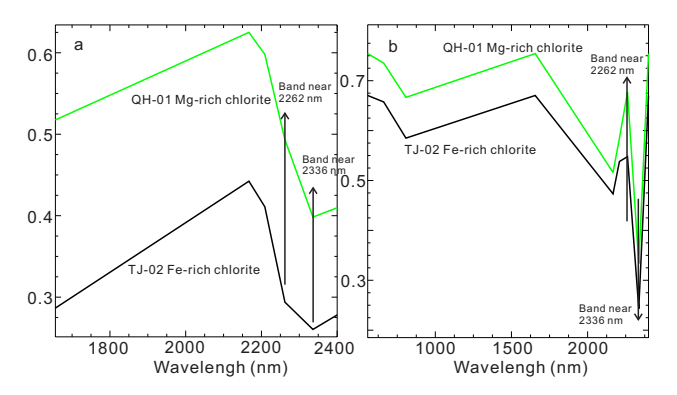


Figure 10: The laboratory and image spectral curves of TJ-02 and QH-01, a is the laboratory spectra resampled to ASTER bands, and b is the image spectra.

for the two hydroxy combination bands are similar, it is possible to distinguish different chlorites using their $\text{Fe}^{2+}/(\text{Fe}^{2+}+\text{Mg})$ values. The frequency of brunsvigite (Ferich chlorite) $(\nu+\delta)_{(AlAl)O-OH}$ absorption should be lower than 4440 cm⁻¹, and the frequency of clinochlore and pycnochlorite (Mg-rich chlorite) $(\nu+\delta)_{(AlAl)O-OH}$ absorption should be higher than 4440 cm⁻¹. In addition, the frequency of brunsvigite (Fe-rich chlorite) $(\nu+\delta)_{(SilAl)O-OH}$ absorption should be lower than 4270 cm⁻¹, and the frequency of clinochlore and pycnochlorite (Mg-rich chlorite) $(\nu+\delta)_{(SiAl)O-OH}$ absorption should be higher than 4270 cm⁻¹.

4 Discussion

Chlorite samples with various Fe-Mg substitutions were studied to establish a correlation between the fundamental vibrations ($\nu_{(AlAl)O-OH}$, $\nu_{(SiAl)O-OH}$, $\delta_{(AlAl)O-OH}$, $\delta_{(SiAl)O-OH)}$ and combination bands (($\nu_{+}\delta$)($\nu_{(AlAl)O-OH)}$) and ($\nu_{+}\delta$)($\nu_{(SiAl)O-OH)}$) of structural OH groups in chlorite min-

erals. Direct linear relations were found between the wavenumbers of the fundamental absorptions and the combination bands, making it possible to identify which stretching and bending bands in the fundamental region form the combination bands in the NIR region in chlorites. It has been shown that these relationships can be used for any other minerals, especially for the OH-bearing minerals and carbonate minerals. The collected and experimental data are well fitted with Eqs. (2) and (3) based on the anharmonic vibration theory. This theory was first used by Petit (2004) [35] in studying first overtones in talcs, whereas we used this method to determine the relation between combination bands and fundamental bands in chlorites for the first time.

From Table 3, the fundamental OH stretching absorption bands of the thirteen samples range from 3567.48 to 3573.53 cm⁻¹ (covering 6.05 cm⁻¹) and from 3442.52 to 3446.66 cm⁻¹ (covering 4.41 cm⁻¹). The OH bending absorption features range from 860.83 to 893.67 cm⁻¹ (covering 32.84 cm⁻¹) and from 749.12 to 787.18 cm⁻¹ (covering 38.06 cm⁻¹). The results of fundamental band positions indicated that the NIR combination band positions might be dominated by OH stretching bands.

The Fe-Mg substitution with $Fe^{2+}/(Fe^{2+}+Mg)$ values between 0.38 to 0.53 at relatively constant $AI^{VI}/(AI^{VI}+Si)$ values ranging from 0.27 to 0.36 was accompanied by both a shift toward lower frequency and a widening of the OH stretching bands. These results confirm the hypothesis of Petit (1999) [30] that OH stretching band frequency is dependent on the amount of Fe-Mg substitution. According to Shirozu (1985) [8], Fe substitution for Mg in chlorites indirectly weakens the surplus negative charge of the surface oxygens and results in an increase of the O-OH distance and further decreases the frequency of the OH stretching band. As the combination band is induced by OH stretching and bending, the NIR OH combination band positions

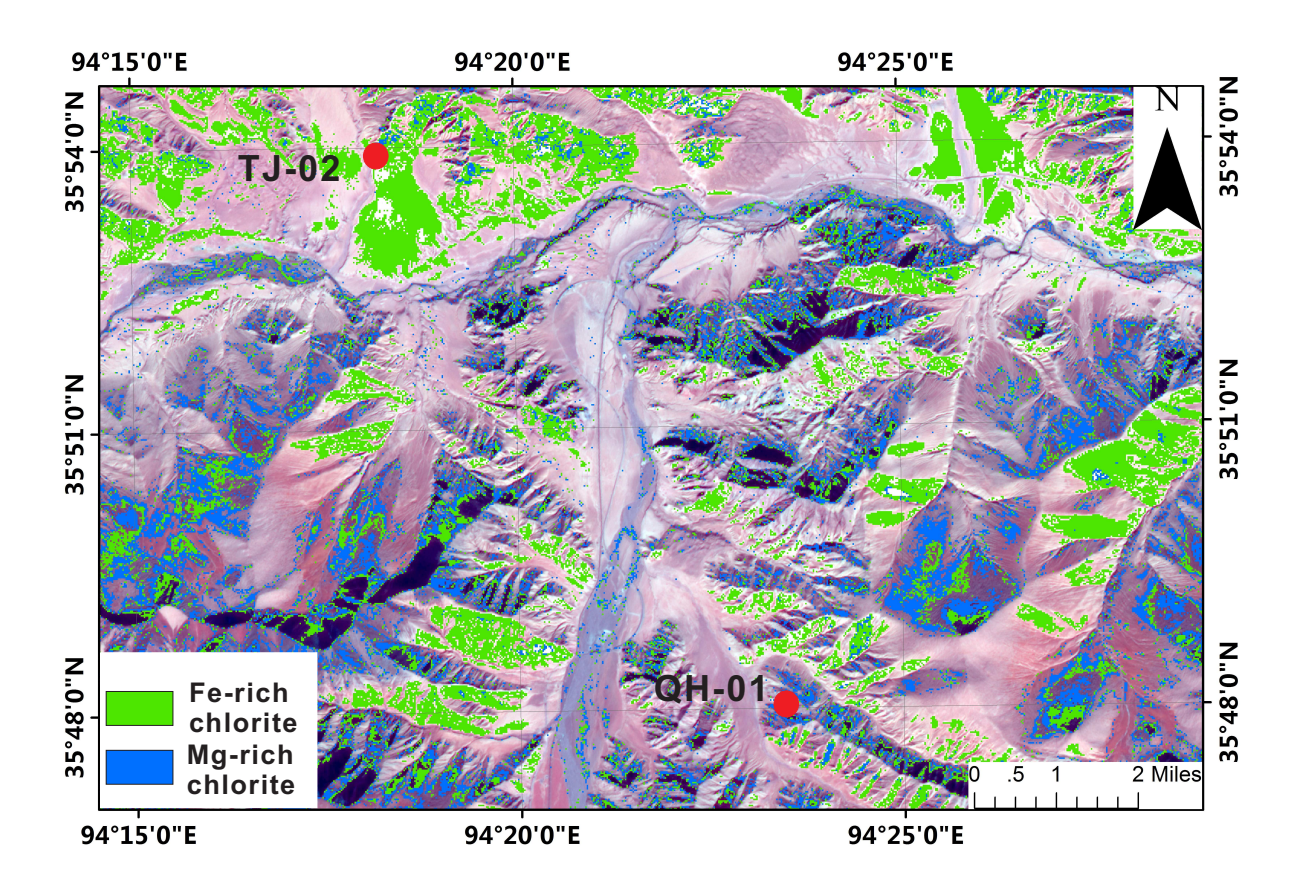


Figure 11: Mapping result of Fe-rich and Mg-rich chlorites using the ASTER data and MF method.

are similarly dependent on the amount of Fe-Mg substitution.

The correlation established above between OH combination bands and fundamental bands provided a technique for determining the cationic environment of the OH group and finding the corresponding OH fundamental bands in the IR region for the interpretation of the OH combination in the NIR region. Compared to Raman spectroscopy, NIR spectroscopy is almost non-destructive, fast, and easy to perform (no preparation of samples) and has a high sensitivity to the hydroxyl group environment. The results clearly show the analytical efficiency of the NIR spectra technique for clay minerals. Nevertheless, the whole interpretation of the observed absorption features needs a further quantitative approach and complementary studies using a rigorous mathematical model. The Infrared spectra of the fundamental vibrations of the OH group could also be added, and the methods developed by Koga (2014) could be applied [38]. However, this method would require considerable knowledge about the components of the samples. Thus, the relationship given above can be generally

applied to better distinguish the presence of certain types of chlorite minerals.

5 Remote Sensing Application

In order to evaluate the feasibility of our findings, the Nachitai area located in east Kunlun Mountains was selected as a test area, where the chlorite minerals are wide spread on the earth's surface. The Advanced Spaceborne Thermal Emission and Reflection Radiometer (ASTER) data was used for detecting the Fe-rich and Mg-rich chlorites. The ASTER satellite carrying the Terra platform (EOS), was launched in December 1999 and provide a finer spectral resolution with three visible and near infrared (VNIR) bands from 520 to 860 nm and six short-wave infrared (SWIR) bands from 1600 to 2500 nm. The ASTER level 1B data used in this study were acquired on 28 October, 2001. The images have been pre-georeferenced to UTM zone 46 North projections with WGS-84 datum. The spatial resolution of SWIR bands were resampled to 15m according

to VNIR bands, and the ASTER data were corrected for atmospheric effects using the Fast Line-of-sight Atmospheric Analysis of Spectral Hypercubes module (FLAASH). Many available studies have successfully used the ASTER data in identifying chlorite minerals from other kinds of minerals including muscovite, calcite, kaolinite and jarosite, but limited literatures reported data and methods could discriminate Mg-rich and Fe-rich chlorite minerals [39–43]. The ASTER data may also provide an opportunity in distinguishing Mg-rich and Fe-rich chlorite minerals due to its finer spectral resolution in SWIR bands and the findings on the spectral features. The traditional mapping method Matched Filtering (MF) was used to distinguish Fe-rich and Mg-rich chlorites. This method have been proved to be a reliable technique in lithological and mineral mapping [44].

The spectral features of different minerals are influenced by atmospheric effects, mineral component, vegetation cover, soil cover, and the spatial and spectral resolution of the image. Even though, the spectral curve of the same target collected from remote sensing images could be significantly different from the laboratory spectra [45]. Two samples of TJ-02 with Fe-rich chlorite and QH-01 contain Mg-rich chlorite were selected, and their laboratory spectra and image spectra were collected respectively. Moreover, the laboratory spectra were resampled according to the ASTER bands. The laboratory spectra resampled to ASTER bands were shown in Figure 9a and the image spectra were shown in Figure 10b. Obviously, the two types of spectra are quite different in shape but the relationship of the absorption depths is similar. The band depths of TJ-02 are deeper than QH-01 in both laboratory and image spectra. This coherence may help remote sensing technique to discriminate Fe-rich and Mg-rich chlorite on the ASTER imagery.

The mapping result of Fe-rich and Mg-rich chlorite using the ASTER data and MF method was showed in Figure 11. This application may be the first test of using the ASTER data to subdivide some different chlorites. This results may help geologists with enriched geological evidence to support some geological findings.

6 Conclusions

The assignment of NIR bands in chlorite spectra and the dominant impact factor of chlorite spectra were achieved by comparing NIR absorption features with Raman absorption features and XRF component results. The application of NIR spectroscopy for the study of chlorites shows great potential for understanding the interactions between the

fundamental absorptions and combinational absorptions. A number of conclusions can be drawn based on the NIR spectra: (a) Chlorites are characterized by two NIR absorptions; the high wavenumber band near 4440 cm $^{-1}$ could be attributed to the combination of (AlAl)O-OH stretching and (AlAl)O-OH bending in the Raman spectra, and the lower wavenumber band near 4263 cm $^{-1}$ could be induced by the combination of (SiAl)O-OH stretching and (SiAl)O-OH bending in the Raman spectra. (b) The positions of the two diagnostic NIR absorptions both have negative correlations with Fe $^{2+}$ /(Fe $^{2+}$ +Mg) values. The NIR absorption features of Fe-rich chlorites may occur at lower frequencies than 4440 cm $^{-1}$ and 4263 cm $^{-1}$, and the NIR absorption features of Mg-rich chlorites may occur at positions higher than these two frequencies.

The interpretation of the NIR spectra of chlorites is also important for mapping hydroxyl-bearing minerals using remotely sensed hyperspectral images and geological field surveys. Spectral analysis with spectral images or field spectrometry is generally used to discriminate compositional variations within altered mineral series, which is important, as mineral composition may systematically vary in an alteration system as a function of the temperature and composition of the hydrothermal fluids and with proximity to zones of mineralization. Mapping these alterations can allow remote sensing researchers and geologists to locate samples within an alteration system to distinguish a certain mineral from other minerals and to define alteration relationships [11, 46, 47]. Accurate interpretations of spectra could contribute to more accurate quantitative analyses of phyllosilicates and to a better understanding of their mineralization relationships.

Acknowledgement: This research was conducted as part of the Fundamental Research Grant Scheme of the National Natural Science Foundation of China (Vote no: 41502312), the Chinese Ministry of Science and Technology (Vote no: 2015BAB05B03-01) and the China Geological Survey Foundation (Vote no: DD20160002 and DD20160336). We are thankful to the State Key Laboratory for Mineral Deposits Research, Nanjing University, the Key Laboratory for Geohazards in Loess Areas, the Chinese Ministry of Natural Resources, the Xi'an Center of China Geological Survey and the Shaanxi Tongguan Observation Base on Geological Environment of Mines for their contributions to this investigation. The authors would like to thank the reviewers for their very helpful and constructive reviews of this manuscript.

References

- Deer, W. A.; Howie, R. A.; Zussman, J. An introduction to the rockforming minerals, 2nd ed.; AW Longman Ltd, Harlow, UK, 1996; pp. 696.
- [2] Kameda, J.; Sugimori, H. Modification to the crystal structure of chlorite during early stages of its dissolution. Phys. Chem. Minerals. 2009, 36, 537-544.
- [3] Kleppe, A. K.; Jephcoat, A. P.; Welch, M. K. The effect of pressure upon hydrogen bonding in chlorite: A raman spectroscopic study of clinochlore to 26.5 GPa. Am. Mineral. 2003, 88, 567-573.
- [4] Tuddenham, W. M.; Lyon, R. J. P. Relation of infrared spectra and chemical analysis from some chlorites and related minerals. Anal. Chem. 1959, 31, 377-380.
- [5] Stubican, V.; Roy, R. Isomorphous substitution and infrared spectra of the layer lattice silicates. Am. Mineral. 1961, 46, 32-51.
- [6] Hayashi, H.; Oinuma, K. Si-O absorption band near 1000 cm-1 and OH absorption bands of chlorite. Am. Mineral. 1967, 52, 1206-1210.
- [7] Shirozu, H. Cation distribution, sheet thickness, and O-OH space in trioctahedral chlorites – an X ray and infrared study. Mineral. J. 1980, 10, 14-34.
- [8] Shirozu, H. Infrared spectra of trioctahedral chlorites in relation to chemical composition. Clay Sci. 1985, 6, 167-176.
- [9] Post, J. L.; Crawford, S. M. Uses of near-infrared spectra for the identification of clay minerals. Appl. Clay Sci. 2014, 95, 383-387.
- [10] Yang, M.; Yang, J.; Ren, G.; Li, J.; Gao, T.; Yi, H.; Han, H.; Zhang, Z.; Liang, N. The application of near-infrared spectral data in studying the chloritized rocks. Infrared Technology and Applications, International Symposium on Optoelectronic Technology and Application 2014, Peking, China, May 13-May 15; SPIE, U.S., 2014; 930025.
- [11] Laakso, K.; Peter, J. M.; Rivard, B.; White, H. P. Short-wave infrared spectral and geochemical characteristics of hydrothermal alteration at the Archean Izok lake Zn-Cu-Pb-Ag volcanogenic massive sulfide deposit, Numavut, Canada: application in exploration target vectoring. Econ. Geol. 2016, 111, 1223-1239.
- [12] Petit, S.; Decarreau, A.; Gates, W.; Andrieux, P.; Grauby, O. Hydrothermal synthesis of dioctahedral smectites: The Al-Fe3+ chemical series. Part II: Crystal-chemistry. Appl. Clay Sci. 2015, 104, 96-105.
- [13] Yang, M.; Ren, G.; Gao, T.; Li, J.; Qiu, D.; Yi, H.; Han, H. Uses of near-infrared spectra for the identification of calcite and dolomite in carbonate rocks. J. Comput. Theor. Nanos. 2015, 12, 5854-5858
- [14] Wu, H.; Wu, G.; Ren, Y.; Yang, L.; Wang, L.; Li, X. Co²⁺/Co³⁺ ratio dependence of electromagnetic wave absorption in hierarchical NiCo₂O₄-CoNiO₂ hybrids. J. Mater. Chem. C. 2015, 29, 7677-7690.
- [15] Wu, H.; Wu, G.; Wang, L. Peculiar porous α -Fe $_2$ O $_3$, γ Fe $_2$ O $_3$ and Fe $_3$ O $_4$ nanospheres: Facile synthesis and electromagnetic properties. Powder Technol. 2015, 269, 443-451.
- [16] Brugge, C. J.; Stiegman, A. E.; Rainen, R. A.; Springsteen, A. W. Use of spectralon as a diffuse reflectance standard for in-flight calibration of earth-orbiting sensors. Optical Engineering, 1993, 32, 805-814.
- [17] Clark, R. N.; Swayze, G. A.; Livo, K. E.; Kokaly, R. F.; King, T. V. V.; Dalton, J. B., Vance, J. S.; Rockwell, B. W.; Hoefen, T.; McDougal, R. R. Surface reflectance calibration of terrestrial imaging spec-

- troscopy data: A tutorial using AVIRIS. The 10th Airborne Earth Science Workshop, Pasadena, U.S., Jet Propulsion Laboratory Publication, 2014, pp. 474.
- [18] G. T. R. Droop. A general equation for estimating Fe3+ concentrations in ferromagnesian silicates and oxides from microprobe analyses, using stoichiometric criteria. Mineralogical Magazine, 1987, 51, 431-435.
- [19] Sunshine, J. M.; Pieters, C. M. Determing the composition of olivine from reflectance spectroscopy. J. Geophys. Res. 1998, 103, 675-688.
- [20] Frost, R. L.; Kloprogge, J. T.; Ding, Z. Near-infrared spectroscopic study of nontronites and ferruginous smectite. Spectrochim. Acta A. 2002, 58, 1657-1688.
- [21] Frost, R. L.; Erickson, K. L.; Adebajo, M. O.; Weier, M. L. Nearinfrared spectroscopy of autunites. Spectrochim. Acta A. 2005, 61, 367-372.
- [22] McKeown, D. A.; Bell, M. I.; Etz, E. S. Vibrational analysis of the dioctahedral mica: 2M1 muscovite. Am. Mineral. 1999, 84, 1041-1048
- [23] Hayashi, H.; Oinuma, K. Relationship between infrared absorption spectra in the region of 450-900 cm-1 and chemical composition of chlorite. Am. Mineral., 1965, 50, 476-483.
- [24] Prieto, A. C.; Lobón, J. M.; Alia, J. M.; Rull, F.; Martin, F. Thermal and spectroscopic analysis of natural trioctahedral chlorites. J. Therm. Anal. 1991, 37, 969-981.
- [25] Shirozu, H. Cation distribution, sheet thickness, and O-OH space in trioctahedral chlorites-An X-ray and infrared study. Miner. J. 1980, 10, 14-34.
- [26] Prieto, A. C.; Dubessy, J.; Cathelineau, M. Structure composition relationships in trioctahedral chlorites: a vibrational spectroscopy study. Clay Clay Miner. 1991, 39, 531-539.
- [27] Kloprogge, J. T.; Frost, R. L.; Rintoul, L. Single crystal raman microscopic study of the asbestos mineral chrysotile. Phys. Chem. Chem. Phys. 1999, 1, 2559-2564.
- [28] Madejova, J.; Komadel, P. Baseline studies of the clay minerals society source clays: infrared methods. Clay Clay Miner. 2001, 49, 410-432.
- [29] Kloprogge, J. T.; Frost, R. L. Thermal decomposition of ferrian chamosite: an infrared emission spectroscopic study. Contrib. Mineral Petrol. 2000, 138, 59-67.
- [30] Petit, S.; Madejová, J.; Decarreau, A.; Martin, E. Characterization of octahedral substitutions in kaolinites using near-infrared spectroscopy. Clay Clay Miner. 1999, 47, 103-108.
- [31] Meer, F. D.; Werff, H. M. A.; Ruitenbeek, F. J. A.; Hecker, C. A.; Bakker, W. H.; Moomen, M. F.; Meijde, M.; Carranza, E. J. M.; Smeth, J. B.; Woldai, T. Multi- and hyperspectral geologic remote sensing: A review. Int. J. Appl. Earth Obs. 2012, 112-128.
- [32] Pour, A. B.; Hashim, M. Hydrothermal alteration mapping from Landsat-8 data, Sar Cheshmeh copper mining district, south-eastern Islamic Republic of Iran. J. T. U. Sci. 2015, 121, 1658-3655.
- [33] Barton, F. E. Theory and principles of near-infrared spectroscopy. Near-Infrared spectroscopy, The 10th International NIR conference, Kyongju-city, Korea, June 10-June 15; International Committee of NIR, 2000.
- [34] Frost, R. L.; Locos, O. B.; Kritof, J.; Kloprogge, J. T. Infrared spectroscopic study of potassium and cesium acetate-intercalated kaolinites. Vibrat. Spectrosc. 2001, 26, 33-42.
- [35] Petit, S.; Decarreau, A.; Martin, F.; Buchet, R. Refined relationship between the position of the fundamental OH stretching and the first overtones for clays. Phys. Chem. Minerals. 2004, 31, 585-

592.

- [36] Guggenheim, S., Adams, J. M., Bain, D. C., Bergaya, F., Brigatti, M. F., Drits, V. A., Formoso, M. L. L., Galan, E., Kogure, T., Stanjek, H. Summary of recommendations of nomenclature committees relevant to clay mineralogy: report of the Association Internationale pour l'Etude des Argiles (AIPEA) Nomenclature Committee for 2006. Clay Minerals. 2006, 41, 863-877.
- [37] Foster, M. D. Interpretation of the composition and a classification of the chlorites. United States Department of the Interior Stewart. Washington, 1962.
- [38] Koga, K. T.; Garrido, C. J.; Padron-Navarta, J. A.; Sanchez-Vizcaino, V. L. FTIR and Raman spectroscopy characterization of fluorinebearing titanian clinohumite in antigorite serpentinite and chlorite harzburgite. Earth Planets Space. 2014, 66, 1-8.
- [39] Rowan, L. C., Mars, J. C. Lithological mapping in the Mountain Pass, California area using Advanced Spaceborne Thermal Emission and Reflection Radiometer (ASTER) data. Remote Sensing of Environment. 2003, 84, 350-366.
- [40] Tommaso, I. D., Rubinstein, N. Hydrothermal alteration mapping using ASTER data in the Infiernillo porphyry deposit, Argentina. Ore Geology Reviews. 2007, 32, 275-290.
- [41] Mars, J. C., Rowan, L. C. Spectral assessment of new ASTER SWIR surface reflectance data products for spectroscopic mapping of rocks and minerals. Remote Sensing of Environment. 2010, 114, 2011-2025.

- [42] Pour, A. B., Hashim, M., Marghany, M. Using spectral mapping techniques on short wave infrared bands of ASTER remote sensing data for alteration mineral mapping in SE Iran. International Journal of the Physical Sciences. 2011, 6, 917-929.
- [43] Pour, A. B., Hashim, M. ASTER, ALI and Hyperion sensors data for lithological mapping and ore minerals exploration. Springer Plus. 2014. 3:130.
- [44] Harris, J. R. et al., Mapping lithology in Canada's Arctic: application of hyperspectral data using the minimum noise fraction transformation and matched filtering. Can. J. Earth Sci. 2005, 42, 2173-2193.
- [45] Yu, L., Porwal, A., Holden, E. J., Dentith, M. C., "Towards automatic lithological classification from remote sensing data using support vector machines", Comput. Gosci., 45, 229-239 (2012).
- [46] Duke, E. F. Near-infrared spectra of muscovite, Tschermak substitution, and metamorphic reaction progress: implications for remote sensing. Geology. 1994, 22, 621-624.
- [47] Young, S. S.; Moon, K. K.; Wang, J. Y. Pyrophyllite mapping in the Nohwa deposit, Korea, using ASTER remote sensing data. Geosci. J. 2014, 18, 295-305.